

---

# MISCLASSIFICATION-AWARE GAUSSIAN SMOOTHING AND MIXED AUGMENTATIONS IMPROVES ROBUSTNESS AGAINST DOMAIN SHIFTS

---

PREPRINT

Athanasios Tsiligkaridis<sup>\*†</sup>, Theodoros Tsiligkaridis<sup>\*‡</sup>

<sup>†</sup>Boston University, Dept. Electrical and Computer Engineering, Boston, MA 02215

<sup>‡</sup>Massachusetts Institute of Technology Lincoln Laboratory, Lexington, MA 02421

<sup>†</sup>atsili@bu.edu, <sup>‡</sup>tsili@mit.edu

June 13, 2022

## ABSTRACT

Deep neural networks achieve high prediction accuracy when the train and test distributions coincide. In practice though, various types of corruptions can deviate from this setup and cause severe performance degradations. Few methods have been proposed to address generalization in the presence of unforeseen domain shifts. In this paper, we propose a misclassification-aware Gaussian smoothing approach, coupled with mixed data augmentations, for improving robustness of image classifiers against a variety of corruptions while still maintaining high clean accuracy. We show that our method improves upon the state-of-the-art in robustness and uncertainty calibration on several image classification benchmarks and network architectures.

## 1 Introduction

Deep neural networks are increasingly being used in computer vision and have achieved state-of-the-art performance on image classification [Krizhevsky et al., 2012, He et al., 2015, Huang et al., 2019]. However, when the test distribution differs from the train distribution, performance can suffer as a result even for mild image corruptions and transformations [Hendrycks and Dietterich, 2019]. In fact, models have unrealistic behavior when faced with out-of-distribution inputs that arise from synthetic corruptions [Hendrycks and Dietterich, 2019], spatial transformations [Engstrom et al., 2019], and data collection setups [Torralba and Efros, 2011, Recht et al., 2019]. Although the mismatch between train and test distributions is common in practice, the problem has not been thoroughly studied yet. Thus, designing models that provide robustness to unforeseen deviations from the train distribution is highly desirable. Furthermore, calibrated uncertainty on test sets associated with a domain shift is also desirable as models can know when mistakes are likely and human-machine teaming can be improved.

The majority of the literature on robustness has focused on adversarial robustness against pixel-level  $\ell_p$  norm-bounded perturbations [Madry et al., 2018, Zhang et al., 2019]. However, the  $\ell_p$  norm-bounded perturbation model for corruptions does not account for common corruptions, such as rotation, translation, blur, compression artifacts, contrast changes, that are often encountered in practice. Semantic perturbations that alter specific attributes of images while still look natural have been also shown to fool classifiers [Joshi et al., 2019, Xiao et al., 2021]. Such domain shifts often correspond to large  $\ell_p$  perturbations that circumvent defenses against imperceptible pixel-level perturbations. Sampling the entire space of possible image variations is not practical to protect models against test time failures, and knowledge of test distribution is not warranted.

The natural approach to defending against a particular fixed distribution shift is to explicitly incorporate such data into the training process, see e.g. [Kang et al., 2019]. However, this paradigm has drawbacks including over-fitting to one type of corruption [Geirhos et al., 2018], e.g., in [Kang et al., 2019] it was shown that  $\ell_\infty$  robustness provides

---

\* Authors have made equal contributions.

poor generalization to unforeseen attacks. Furthermore, the empirical study in [Chun et al., 2019] shows that several expensive methods improve robustness at the cost of lower clean accuracy or degraded uncertainty estimation and there are large trade-offs for a variety of regularization methods. Data augmentation policies have been proposed to increase clean accuracy [Cubuk et al., 2019] based on reinforcement learning but are computationally expensive. Uncertainty calibration can be improved by simple ensembles [Lakshminarayanan et al., 2017] and pre-training [Hendrycks et al., 2019]. However, it has been shown that calibration degrades significantly under domain shifts [Ovadia et al., 2019].

Recent work [Hendrycks et al., 2020] proposed randomized and diverse augmentations coupled with a consistency loss to improve robustness and uncertainty calibration against corruptions while maintaining clean accuracy. However, nontrivial accuracy and uncertainty calibration gaps still remain between the clean and corrupt setting, and it remains an open question to close these gaps.

In this work, we propose a misclassification-aware training technique based on loss landscape smoothing at multiple scales and enforcing consistency between clean examples and mixed data augmentations, generated from a set of primitive augmentations, to improve robustness and uncertainty calibration of image classifiers in the presence of unforeseen domain shifts. Our approach can be characterized as a type of data augmentation strategy coupled with adaptive consistency regularization. Another way to interpret our approach is through the lens of local smoothing as part of our proposed consistency regularization induces a smoothing and flattening effect on the local loss landscape. Our experimental results show that our modeling technique produces models that are highly resistant to a variety of practical distribution shifts.

Our contributions are summarized below:

- We introduce a misclassification-aware consistency loss, coupled with diverse Gaussian noise and mixed augmentations, and a corresponding training algorithm (MAGNMA).
- We provide an analysis for diverse Gaussian noise regularization that uncovers an inducing effect of smoothing and flattening of the local loss landscape.
- We experimentally show the efficacy of our approach on common image corruptions for CIFAR-10-C and CIFAR-100-C datasets and several network architectures.
- We show our approach outperforms competitive baselines in term of robustness and improved uncertainty calibration in the presence of common image corruptions.

## 2 Background and Related Work

We assume labeled data of the form  $(x, y) \sim \mathcal{D}$  drawn from distribution  $\mathcal{D}$ . The labels  $y$  correspond to  $C$  classes. Neural network function  $f_\theta(\cdot)$  maps inputs into logits, and  $\theta$  are the model parameters. The softmax layer is used to map logits into class probability scores given by  $p_c(x) = e^{f_{\theta,c}(x)} / \sum_l e^{f_{\theta,l}(x)}$ .

**Standard Training.** The standard criterion for training deep neural networks is empirical risk minimization (Standard):

$$\min_{\theta} \mathbb{E}_{(x,y) \sim \mathcal{D}} [\mathcal{L}(f_\theta(x), y)] \quad (1)$$

where the loss is chosen to be the cross-entropy function  $\mathcal{L}(f_\theta(x), y) = -y^T \log p_\theta(x)$ . While training using the criterion (1) yields high accuracy on clean test sets, the network generalization performance to a variety of data shifts may suffer.

**Adversarial Training against  $\ell_p$  Adversary.** Adversarial training (AT) [Madry et al., 2018] is one of the most effective defenses against  $\ell_p$  norm-bounded perturbations which minimizes the adversarial risk,

$$\min_{\theta} \mathbb{E}_{(x,y) \sim \mathcal{D}} \left[ \max_{\|\delta\|_p \leq \epsilon} \mathcal{L}(f_\theta(x + \delta), y) \right] \quad (2)$$

During the training process, adversarial attacks are computed at inputs  $x$  that solve the inner maximization problem. The inner maximization may be solved iteratively using projected gradient descent (PGD) for norms  $p \in \{2, \infty\}$ , i.e.,  $\delta^{(k+1)} = \mathcal{P}_{B_p(\epsilon)}(\delta^{(k)} + \alpha \nabla_{\delta} \mathcal{L}(x + \delta^{(k)}, y))$  where  $\mathcal{P}_{B_p(\epsilon)}(z) = \arg \min_{u \in B_p(\epsilon)} \|z - u\|_2^2$  is the orthogonal projection onto the constraint set. Another robust training approach that trades-off the natural and robust error using smoothing is TRADES [Zhang et al., 2019]:

$$\min_{\theta} \mathbb{E}_{(x,y) \sim \mathcal{D}} \left[ \mathcal{L}(f_\theta(x), y) + \lambda \max_{\|\delta\|_p \leq \epsilon} D(p(x; \theta) \| p(x + \delta; \theta)) \right] \quad (3)$$

where  $D$  denotes the Kullback-Leibler divergence  $D(p \parallel q) = \sum_c p_c \log \frac{p_c}{q_c}$  and the inner maximization is computed using PGD.

These robust methods optimize robustness only inside the  $\epsilon$ -ball of the training distribution which does not capture *perceptible* data shifts such as common image corruptions [Hendrycks and Dietterich, 2019]. Training with arbitrarily large  $\epsilon$  in the pixel-wise robustness formulations fails in practice as image quality degrades and clean accuracy suffers due to inherent tradeoff [Tsipras et al., 2019].

**Random Self-Ensemble Training.** In the context of adversarial robustness, a random self-ensemble (RSE) method has been proposed [Liu et al., 2018] based on noise injection at the input layer and each layer of neural networks and was demonstrated to provide good levels of robustness against white-box attacks. Considering noise at the input layer only, the RSE training criterion is:

$$\min_{\theta} \mathbb{E}_{(x,y) \sim \mathcal{D}} \left[ \mathbb{E}_{\delta \sim \mathcal{N}(0, \sigma^2 I)} \mathcal{L}(f_{\theta}(x + \delta), y) \right] \quad (4)$$

and predictions are ensembled at inference time as  $\hat{y}(x) = \arg \max_c \frac{1}{n} \sum_{i=1}^n p_c(x + \delta_i)$  where  $\delta_i \sim \mathcal{N}(0, \sigma^2 I)$ . This increases inference time due to the ensemble, is prone to overfitting at a fixed noise level  $\sigma$ , and cannot handle certain real-world corruptions well, such as contrast and fog.

**Diverse Data Augmentation Training.** A recently proposed data augmentation technique, AugMix [Hendrycks et al., 2020], was shown to achieve SOTA performance against unforeseen corruptions by enforcing a consistency loss coupled with a data augmentation scheme:

$$\min_{\theta} \mathbb{E}_{(x,y) \sim \mathcal{D}} \left[ \mathcal{L}(f_{\theta}(x), y) + \lambda JS(p_{\theta}(x); p_{\theta}(x_{a,1}); p_{\theta}(x_{a,2})) \right] \quad (5)$$

where  $JS(p_1; p_2; p_3) = \frac{1}{3}(D(p_1 \parallel p_{\text{mix}}) + D(p_2 \parallel p_{\text{mix}}) + D(p_3 \parallel p_{\text{mix}}))$  is the Jensen-Shannon divergence,  $p_{\text{mix}} = \frac{1}{3}(p_1 + p_2 + p_3)$ , and  $x_{a,1}, x_{a,2}$  are augmented variants of  $x$  formed by mixing composition chains each consisting of a finite number of augmentation operations chosen from the set  $\{\text{rotate}, \text{posteriorize}, \text{shear-x}, \text{shear-y}, \text{translate-x}, \text{translate-y}, \text{solarize}, \text{equalize}, \text{autocontrast}\}$ . Using diversity and randomness in choosing these operations and mixing weights at different levels of severity during training, this data augmentation method is empirically shown to significantly improve robustness against unforeseen corruptions in comparison to CutOut [DeVries and Taylor, 2017], MixUp [Zhang et al., 2017, Tokozume et al., 2018], CutMix [Yun et al., 2019], and AutoAugment [Cubuk et al., 2018] schemes. While this baseline offers strong performance, it still has difficulty dealing with certain noise and blur-based corruptions and can be further improved upon.

### 3 Misclassification-Aware Gaussian Noise Smoothing with Mixed Augmentations Training

Our goal is to design a training method to improve generalization against a variety of corruptions while fitting in existing pipelines with minimal changes. Our idea consists of introducing a misclassification-aware consistency loss that embeds representations of clean data samples and diversified noise-corrupted or mixed augmentation-corrupted versions similarly. These consistency losses are described below:

- (a) We encourage data embeddings of clean examples  $x$  and noisy samples  $x + \delta$  to be similar. To increase resiliency against a variety of Gaussian noise distributions, we diversify the perturbation statistics by choosing a random noise level  $\sigma$  uniformly in the range  $[0, \sigma_{\text{max}}]$  and then generating the random perturbation  $\delta$ .
- (b) We encourage data embeddings of clean examples  $x$  and mixed augmentations  $x_a(w) = wx + (1 - w)T_a(x)$  to be similar. Here  $T_a(x)$  is generated by applying  $x$  to one of the randomly chosen augmentations  $a$  from the set  $\mathcal{A} = \{\text{autocontrast}, \text{equalize}, \text{posteriorize}, \text{solarize}\}$  where each one can be applied with a varying discrete intensity level  $u$  ranging from 1 to 10.

Weighting is also applied using the *true class confidence* level  $[p_{\theta}(x)]_y$  which allows for the network training to adaptively increase regularization on high-confidence correct predictions and focus more on the classification loss when the predictions are incorrect.

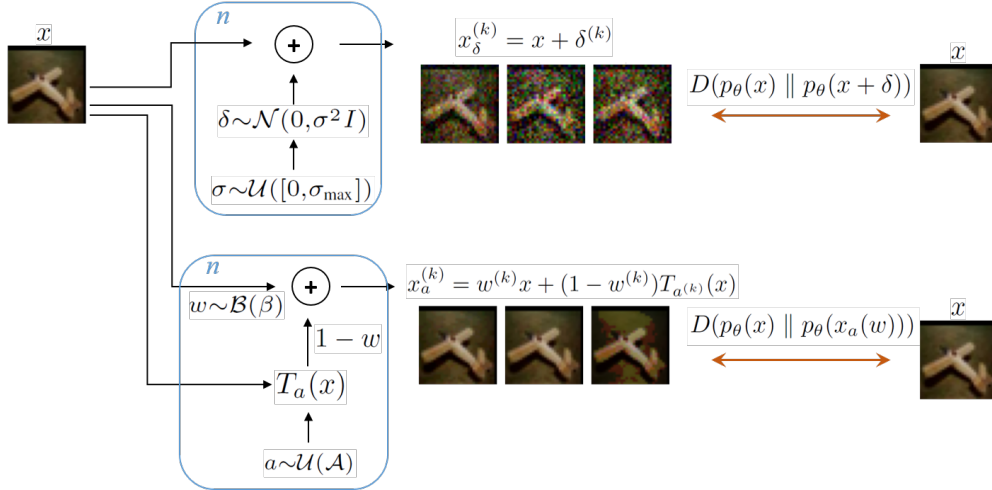


Figure 1: An illustration of our MAGNMA training methodology. During training, input images  $x$  are fed into two separate branches each consisting of generating  $n$  samples. The top branch adds Gaussian noise  $\delta$  to clean images controlled by a variety of scales  $\sigma$  sampled from a uniform distribution, and a consistency loss wrt. the clean images is formed. The bottom branch constructs mixed augmentations by linearly mixing clean images  $x$  and transformed images  $T_a(x)$  generated by applying augmentations  $a$  randomly chosen from a set  $\mathcal{A}$ , from which another consistency loss wrt. clean images is formed.

Our proposed training criterion is:

$$\begin{aligned} \min_{\theta} \mathbb{E}_{(x,y) \sim \mathcal{D}} [\mathcal{L}(f_\theta(x), y) \\ + \lambda_1 [p_\theta(x)]_y \mathbb{E}_{\sigma \sim \mathcal{U}([0, \sigma_{\max}])} \mathbb{E}_{\delta \sim \mathcal{N}(0, \sigma^2 I)} D(p_\theta(x) \parallel p_\theta(x + \delta)) \\ + \lambda_2 [p_\theta(x)]_y \mathbb{E}_{a \sim \mathcal{U}(\mathcal{A})} \mathbb{E}_{w \sim \mathcal{B}(\beta)} D(p_\theta(x) \parallel p_\theta(x_a(w)))] \end{aligned} \quad (6)$$

The classification loss  $\mathcal{L}(f_\theta(x), y)$  in (6) maximizes accuracy on clean examples, while the consistency regularization terms force clean and randomly corrupted examples (Gaussian noise or mixed from a small finite augmentation set) to have similar output distributions. Here,  $\lambda_1, \lambda_2 \geq 0$  are regularization parameters,  $\mathcal{U}$  denotes uniform distribution,  $\mathcal{N}(0, \sigma^2 I)$  denotes the normal distribution with standard deviation  $\sigma$ ,  $\mathcal{B}(\beta)$  denotes Beta distribution with equal shape parameters  $\beta$  and probability density function  $p(w; \beta) = \frac{\Gamma(2\beta)}{\Gamma(\beta)^2} w^{\beta-1} (1-w)^{\beta-1}$ .

We call our approach (6) Misclassification-Aware Gaussian Noise smoothing with Mixed Augmentations, MAGNMA, and Algorithm 1 depicts our training procedure. A sample-based approximation is used to approximate the regularizers to maintain low computational complexity during training. In practice, a couple samples suffice to obtain strong robustness and uncertainty calibration. The concept is graphically illustrated in Figure 1.

The motivation for placing distributions on scales  $\sigma$  and associated noise perturbations  $\delta$ , the mixing weights  $w$ , augmentations  $a$  and associated intensity levels  $u$  to approximate (6) is to avoid memorization of fixed augmentations [Geirhos et al., 2018] which leads to poor generalization against a variety of domain shifts. In contrast to RSE (4) we use a diverse set of Gaussian noise scales and do not rely on test-time ensembling. In contrast to AugMix (5), the second regularizer in (6) includes true class confidence weighting, leverages the Kullback-Leibler divergence instead of Jensen-Shannon divergence for consistency loss, and uses only one mixing chain with a single random augmentation operation sampled from a smaller set of augmentations  $\mathcal{A}$ . Thus, while our second regularizer uses less diverse augmentation than AugMix, coupling this with misclassification-aware weighting and Gaussian smoothing provides improved robustness and uncertainty calibration in the presence of domain shifts.

Interestingly, training with diverse Gaussian noise augmentations coupled with misclassification-aware weighting provides robustness not only against Gaussian noise but also against a variety of weather, blur, noise and digital corruptions, as evidenced in our results. Furthermore, training with misclassification-aware mixed augmentation consistency regularization also provides a high level of corruption robustness.

---

**Algorithm 1** MAGNMA pseudocode
 

---

Input: Training data  $\{(x_i, y_i)\}$ , Network  $f_\theta$ , Training epochs  $T$ , Batch size  $|B|$ , learning rate schedule  $\eta_t$ ,  $n$  samples, hyperparameters  $(\lambda_1, \lambda_2, \sigma_{\max}, \beta)$   
 Result: Trained network  $f_\theta$   
**for**  $t=0$  to  $T-1$  **do**  
   **for** each batch  $(x, y) \sim \mathcal{D}$  **do**  
     **for** sample  $k \in \{1, \dots, n\}$  **do**  
       Generate  $\sigma^{(k)} \sim \mathcal{U}(0, \sigma_{\max})$  for each example  
       Generate  $\delta^{(k)} \sim \mathcal{N}(0, (\sigma^{(k)})^2 I)$  for each example  
        $x_\delta^{(k)} = x + \delta^{(k)}$   
     **end for**  
      $R(x_i) = \frac{1}{n} \sum_{k=1}^n D(p_\theta(x_i) \parallel p_\theta(x_{i,\delta}^{(k)}))$   
     **for** sample  $k \in \{1, \dots, n\}$  **do**  
       Generate  $a^{(k)} \sim \mathcal{U}(\mathcal{A})$  for each example and apply augmentation to  $x$  to form  $T_{a^{(k)}}(x)$   
       Generate  $w^{(k)} \sim \mathcal{B}(\beta)$  for each example  
        $x_a^{(k)} = w^{(k)}x + (1 - w^{(k)})T_{a^{(k)}}(x)$   
     **end for**  
      $Z(x_i) = \frac{1}{n} \sum_{k=1}^n D(p_\theta(x_i) \parallel p_\theta(x_{i,a}^{(k)}))$   
      $\mathcal{L}_T(x_i, y_i) = \mathcal{L}(x_i, y_i) + \lambda_1 [p_\theta(x_i)]_{y_i} R(x_i) + \lambda_2 [p_\theta(x_i)]_{y_i} Z(x_i)$   
      $\theta = \theta - \eta_t \frac{1}{|B|} \sum_{i \in B} \nabla_\theta \mathcal{L}_T(x_i, y_i)$   
   **end for**  
**end for**

---

### 3.1 Analysis of Gaussian Noise Consistency Regularization

In this section, we analyze the effect of Gaussian noise regularization in the small-noise regime. Specifically, we obtain a relationship between loss curvature and Fisher information which is further used to derive a bound on the local loss deviation in a neighborhood of data examples. This bound is used to understand the effect of the Gaussian noise regularizer on the local loss landscape and motivate our misclassification-aware modification.

Using a second-order Taylor expansion on the KL divergence, for small  $\sigma$  [Kullback, 1997]:

$$D(p_\theta(x) \parallel p_\theta(x + \delta)) \approx \frac{1}{2} \delta^T G_\theta(x) \delta$$

where  $G_\theta(x)$  is the Fisher information matrix (FIM) given by:

$$G_\theta(x) = \sum_k [p_\theta(x)]_k \nabla_x \log[p_\theta(x)]_k (\nabla_x \log[p_\theta(x)]_k)^T \quad (7)$$

Taking the expectation,

$$\mathbb{E}_{\delta \sim \mathcal{N}(0, \sigma^2 I)} D(p_\theta(x) \parallel p_\theta(x + \delta)) = \frac{\sigma^2}{2} \text{Tr}(G_\theta(x)) \quad (8)$$

where we used  $\mathbb{E}_{\delta \sim \mathcal{N}(0, \sigma^2 I)} [\delta \delta^T] = \sigma^2 I$ . Taking the outer expectation wrt.  $\sigma$  on approximation (8):

$$\begin{aligned}
 & \mathbb{E}_{\sigma \sim \mathcal{U}([0, \sigma_{\max}])} \mathbb{E}_{\delta \sim \mathcal{N}(0, \sigma^2 I)} D(p_\theta(x) \parallel p_\theta(x + \delta)) \\
 & \approx \mathbb{E}_{\sigma \sim \mathcal{U}([0, \sigma_{\max}])} \left[ \frac{\sigma^2}{2} \right] \text{Tr}(G_\theta(x)) \\
 & = \frac{\sigma_{\max}^2}{6} \text{Tr}(G_\theta(x)) \quad (9)
 \end{aligned}$$

The FIM has a strong connection to curvature; in fact for the case of cross-entropy, the Hessian matrix of the loss function is identical to the FIM (7), as the next proposition shows.

**Proposition 1.** *The following relation holds  $H(x) := \nabla_x^2 \mathcal{L}(f_\theta(x), y) = G_\theta(x)$ .*

Thus, minimizing with the Gaussian noise regularizer (9) is equivalent to minimizing the curvature in all directions equally since  $\text{Tr}(H(x)) = \sum_i \lambda_i(H(x))$  where  $\lambda_i$  denote the sorted Hessian eigenvalues. This has the effect of inducing low curvature in the loss landscape of  $\mathcal{L}$  around  $x$  and encourages a locally linear behavior.

What we show next is that there is another interesting effect that the KL smoothing regularizer induces. Substituting (7) into (9) and simplifying, we obtain:

$$\begin{aligned} & \mathbb{E}_{\sigma \sim \mathcal{U}([0, \sigma_{\max}])} \mathbb{E}_{\delta \sim \mathcal{N}(0, \sigma^2)} D(p_\theta(x) \parallel p_\theta(x + \delta)) \\ & \approx \frac{\sigma_{\max}^2}{6} \sum_k [p_\theta(x)]_k \|\nabla_x \log[p_\theta(x)]_k\|_2^2 \end{aligned} \quad (10)$$

This can be interpreted a regularization term that induces stability of predictions within a local neighborhood of  $x$  through weighted logit smoothing. This type of weighted logit smoothing leads to a bound on the local loss deviation.

**Theorem 1.** *The following bound holds on the loss function:*

$$|\mathcal{L}(x + \delta, y) - \mathcal{L}(x, y)| \leq \|\delta\|_2 \cdot \sqrt{\sum_k y_k \|\nabla_x \log p(x)_k\|_2^2} + \frac{1}{2} \lambda_{\max}(H(x)) \|\delta\|_2^2 + o(\|\delta\|_2^2) \quad (11)$$

A consequence of Theorem 1 is that for correct classifications where  $y_k \approx p(x)_k$ , minimizing the regularizer (10) has a twofold effect: (a) curvature is minimized, as the Hessian trace upper bounds the maximum Hessian eigenvalue of the loss  $\mathcal{L}(x, y)$ ,  $\lambda_{\max}(H(x)) \leq \text{Tr}(H(x))$ , and (b) loss surface flatness is increased by minimizing the norm of the loss gradient,  $\|\nabla_x \mathcal{L}(x, y)\|_2$ . Thus, we choose to include the effect of *true class confidence* in this regularizer as shown in the second term of (6) via multiplication with  $p(x)_y$ . This adapts the regularization strength making this regularizer misclassification-aware. For higher confidence examples, the Gaussian smoothing effect increases to make the loss more locally regular, while for misclassifications this effect is minimized to focus the learning on the classification loss.

## 4 Experimental Results

**Datasets.** The datasets used in this experimental results are CIFAR-10 and CIFAR-100 [Krizhevsky et al., 2009], both containing color images of size  $32 \times 32 \times 3$  spanned across 50,000 train images and 10,000 test images. Robustness against data shifts is measured by evaluating on CIFAR-10-C and CIFAR-100-C respectively [Hendrycks and Dietterich, 2019]. Each of these corrupted datasets contain a total of  $M = 18$  corruptions at  $J = 5$  severity levels. The ‘gaussian noise’ corruption is excluded from our evaluations.

**Computing infrastructure.** All experiments were performed using 2 Volta V100 GPUs and 4 CPU cores. Methods were all implemented using the PyTorch deep learning framework.

**Baselines.** The baseline methods considered include standard training (Standard), adversarial training (AT), tradeoff-inspired adversarial defense via surrogate-loss minimization (TRADES), random self-ensemble (RSE), diverse augmentation mixing chains (AugMix). The adversarial models based on AT and TRADES were trained against an  $\ell_\infty$  adversary using  $\epsilon = 8/255$  and 7 PGD steps with step size  $2.5\epsilon/7$  to allow sufficient exploration of the constraint set’s boundary.

Another related baseline we consider is training with diverse Gaussian noise augmentations denoted as Gaussian Noise (GN) training:

$$\min_{\theta} \mathbb{E}_{(x, y) \sim \mathcal{D}} \left[ \mathbb{E}_{\sigma \sim \mathcal{U}([0, \sigma_{\max}])} \mathbb{E}_{\delta \sim \mathcal{N}(0, \sigma^2 I)} \mathcal{L}(f_\theta(x + \delta), y) \right] \quad (12)$$

**Training Details.** The MAGNMA training method is demonstrated on deep residual network architecture ResNet-18 [He et al., 2016], densely connected convolutional architecture DenseNet-121 [Huang et al., 2017], and Inception-V3 [Szegedy et al., 2015]. The learning rate is started at 0.1 and decays every 50 epochs by a factor of 10. Pre-processing steps include standard random cropping, random horizontal flips, color jitter (0.25) and random rotation (2 degrees).

Training was performed for 150 epochs using SGD with Nesterov momentum 0.9 and weight decay 0.0005. The model with the highest clean accuracy computed on the test set was selected as the best performer. For each performance metric, the mean and standard deviation accuracy over 3 independently trained model runs is reported.

For RSE, a noise standard deviation  $\sigma = 0.1$  was chosen to achieve a high mCA experimentally with  $n = 10$  samples used in test-time ensembling. For AugMix,  $\lambda = 12$  was chosen as in the original implementation.

For MAGNMA, parameters  $\sigma_{\max} = 0.2$ ,  $\beta = 1$  were used for all experiments with  $\lambda_1 = 0.2$  and  $\lambda_2 = 0.3$ . For shorthand, ablation variants of MAGNMA with (a)  $\lambda_1 > 0$ ,  $\lambda_2 = 0$ , (b)  $\lambda_1 = 0$ ,  $\lambda_2 > 0$ , (c)  $\lambda_1 > 0$ ,  $\lambda_2 > 0$  are denoted as (a)MAGNMA $\bullet\circ$ , (b)MAGNMA $\circ\bullet$ , (c)MAGNMA $\bullet\bullet$ , respectively.

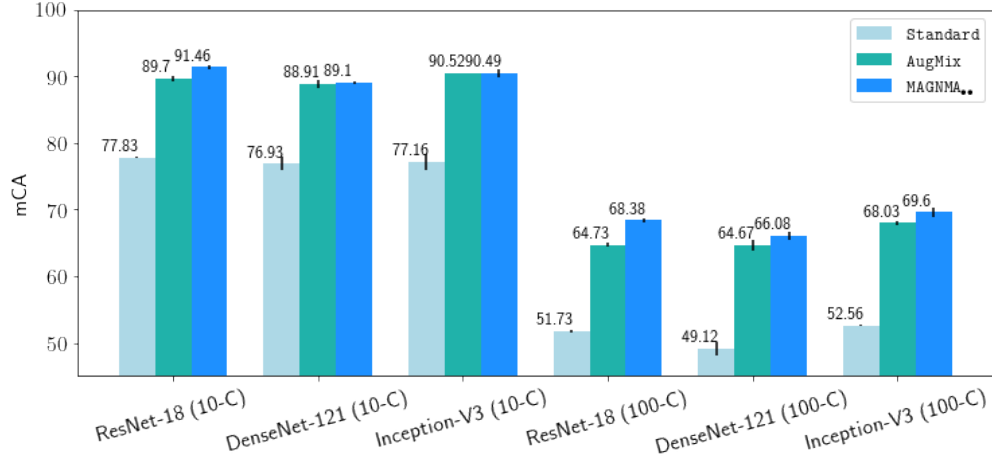


Figure 2: Robustness results showing mCA for multiple network architectures on CIFAR-10-C and CIFAR-100-C datasets. Our proposed method MAGNMA achieves the largest mCA score for nearly all architectures.

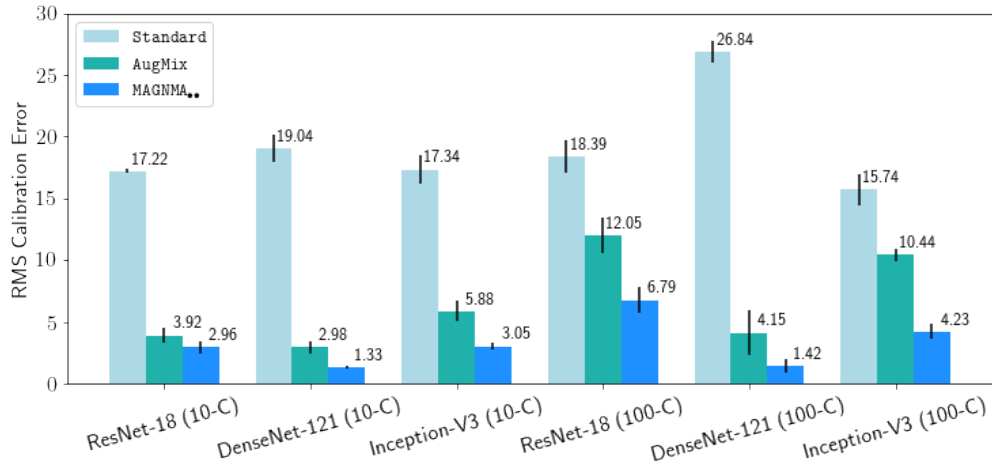


Figure 3: RMS calibration error for multiple network architectures on CIFAR-10-C and CIFAR-100-C datasets. Our proposed method MAGNMA achieves the smallest calibration error for all architectures.

**Performance Metrics.** Classification performance on the clean dataset is measured using test accuracy, i.e.,  $\frac{1}{n} \sum_{i=1}^n \mathbb{1}_{\{y_i = \hat{y}_i\}}$ . Robustness against domain shifts is measured using accuracy on a corrupted validation set for different severity levels  $j$ . For a specific corruption type  $m \in \{1, \dots, M\}$  and severity level  $j \in \{1, \dots, J\}$ , let  $A_{m,j}$  denote the corresponding accuracy. The *mean corruption accuracy (mCA)* is defined as:  $A_M = \frac{1}{MJ} \sum_{m=1}^M \sum_{j=1}^J A_{m,j}$ .

Classifier calibration refers to the problem of true empirical correct likelihood matching the predicted confidence metric. This leads to trustworthy probability estimates of the model predictions. Uncertainty calibration performance is measured using the root-mean-square (RMS) calibration. Consider a partition of  $n_B$  bins  $\{B_i\}$  that corresponding to increasing levels of confidence. Then, RMS calibration error, which measures the discrepancy between the empirical accuracy and the prediction confidence level, is computed as:  $E_c = \sqrt{\sum_{i=1}^{n_B} \frac{|B_i|}{n} \left( \frac{1}{|B_i|} \sum_{j \in B_i} \mathbb{1}_{\{y_j = \hat{y}_j\}} - \frac{1}{|B_i|} \sum_{j \in B_i} c_j \right)^2}$ .

**Robustness Results.** Classification accuracy results computed on the clean and corrupted CIFAR-10 test sets are shown in Table 3 for a variety of deep learning methods on the ResNet-18 architecture. In comparison to the 'Standard' baseline trained with (1), our misclassification-aware Gaussian noise smoothing coupled with mixed augmentations (MAGNMA) achieves 13.6% mCA absolute improvement, outperforming the previous SOTA method AugMix which obtained a smaller 11.9% improvement, adversarial training and random self-ensemble baselines by a significant margin. Ablation variants of MAGNMA where the mixed augmentation/Gaussian noise regularizer is inactive yields 9.3% and

11.8% mCA improvement over standard training respectively. In particular, MAGNMA achieves the best corrupt accuracy for the majority of corruptions, except for a few for which AugMix slightly improves in mean. We remark that MAGNMA achieves similar corrupt accuracies within the standard deviation. We further note that MAGNMA maintains a high clean accuracy, unlike the adversarial training methods AT and TRADES, and does not require ensembling at test time as in RSE. Including both the Gaussian noise and mixed augmentation consistency losses regularizes the model in complementary ways and improves generalization to a variety of corruptions. A general observation we make from the ablation MAGNMA variants is that regularizing the classification loss with the Gaussian noise consistency term tends to improve robustness in the presence of digital noise corruptions, while the mixed augmentation consistency term tends to improve robustness against blur and contrast corruptions. Hyperparameters were experimentally chosen to achieve a high mCA score (see Supplementary Material for sensitivity analysis).

Classification accuracy results on clean and corrupted CIFAR-100 test sets are shown in Table 4 for various baselines on ResNet-18. Similar trends are observed with our proposed MAGNMA method achieving 16.7% mCA absolute improvement, thus improving upon all baselines, including AugMix. Ablation variants of MAGNMA with mixed augmentation/Gaussian regularizer being inactive yield 10.8% and 14.0% mCA improvements, respectively, over Standard training.

Classification accuracy results on multiple network architectures are shown in Table 2 and Figure 2, which continue to support that MAGNMA achieves SOTA performance on CIFAR-10-C and CIFAR-100-C with average mCA improvements of 13.0% and 16.9%, respectively, over Standard training.

**Uncertainty Calibration Results.** Calibration performance is measured on the clean and corrupted CIFAR-10 validation sets on different model architectures, as shown in Table 1 and Figure 3. MAGNMA offers significant improvements in RMSE calibration errors over Standard training; specifically, an average absolute improvement in RMSE calibration error of 15.4% and 16.2% on the corrupted CIFAR-10-C and CIFAR-100-C validation sets, respectively. Furthermore, in comparison to AugMix, MAGNMA achieves 2.81% and 4.73% absolute RMSE calibration error improvement for CIFAR-10-C and CIFAR-100-C, respectively.

| Architecture | Test Set    | Standard   | AugMix     | MAGNMA <sub>••</sub> |
|--------------|-------------|------------|------------|----------------------|
| ResNet-18    | CIFAR-10    | 5.17±0.43  | 1.60±0.29  | 1.69±0.04            |
|              | CIFAR-10-C  | 17.22±0.15 | 3.92±0.63  | <b>2.96±0.47</b>     |
| DenseNet-121 | CIFAR-10    | 5.91±0.42  | 2.77±0.29  | 2.69±0.40            |
|              | CIFAR-10-C  | 19.04±1.07 | 2.98±0.50  | <b>1.33±0.11</b>     |
| Inception-V3 | CIFAR-10    | 5.24±0.19  | 1.88±0.14  | 1.46±0.31            |
|              | CIFAR-10-C  | 17.34±1.15 | 5.88±0.83  | <b>3.05±0.29</b>     |
| ResNet-18    | CIFAR-100   | 7.70±0.42  | 4.41±0.94  | 2.82±0.42            |
|              | CIFAR-100-C | 18.39±1.35 | 12.05±1.43 | <b>6.79±1.04</b>     |
| DenseNet-121 | CIFAR-100   | 11.91±0.67 | 3.15±0.87  | 5.41±0.74            |
|              | CIFAR-100-C | 26.84±0.87 | 4.15±1.82  | <b>1.42±0.54</b>     |
| Inception-V3 | CIFAR-100   | 6.50±0.48  | 4.59±0.62  | 4.01±0.42            |
|              | CIFAR-100-C | 15.74±1.25 | 10.44±0.48 | <b>4.23±0.6</b>      |

Table 1: RMS calibration error (percentage) on CIFAR-10/CIFAR-10-C and CIFAR-100/CIFAR-100-C datasets on ResNet-18, DenseNet-121 and Inception-V3 architectures. MAGNMA achieves a large/moderate reduction in RMSE calibration error in comparison to Standard/AugMix training.

## 5 Limitations

Our focus in this work is designing deep image classifiers that are robust to various image corruptions at different levels of severity. In addition, we offer a motivation for misclassification-aware Gaussian smoothing through a loss landscape analysis. Future work may focus on extending this methodology to data modalities beyond vision and measuring robustness performance.

## 6 Conclusion

In this paper, a regularization method for training robust deep learning classifiers is presented based on misclassification-aware Gaussian smoothing at different scales and mixed augmentations. We empirically show that our training method yields state-of-the-art robustness and uncertainty calibration under unforeseen domain shifts, for different network architectures and datasets. We hope this work encourages more research on improving generalization of classifiers against natural occurring corruptions and other distribution shifts.

| Architecture | Test Set    | Standard   | AugMix             | MAGNMA <sup>••</sup> |
|--------------|-------------|------------|--------------------|----------------------|
| ResNet-18    | CIFAR-10    | 94.79±0.47 | 95.33±0.40         | 95.14±0.17           |
|              | CIFAR-10-C  | 77.83±0.11 | 89.70±0.40         | <b>91.46</b> ±0.28   |
| DenseNet-121 | CIFAR-10    | 94.40±0.33 | 95.20±0.37         | 94.04±0.23           |
|              | CIFAR-10-C  | 76.93±1.01 | 88.91±0.59         | <b>89.10</b> ±0.25   |
| Inception-V3 | CIFAR-10    | 94.59±0.50 | 96.10±0.19         | 95.02±0.36           |
|              | CIFAR-10-C  | 77.16±1.21 | <b>90.52</b> ±0.06 | 90.49±0.56           |
| ResNet-18    | CIFAR-100   | 76.60±0.15 | 76.44±0.34         | 76.79±0.07           |
|              | CIFAR-100-C | 51.73±0.27 | 64.73±0.28         | <b>68.38</b> ±0.23   |
| DenseNet-121 | CIFAR-100   | 75.20±0.93 | 77.14±0.99         | 75.84±0.39           |
|              | CIFAR-100-C | 49.12±0.99 | 64.67±0.84         | <b>66.08</b> ±0.57   |
| Inception-V3 | CIFAR-100   | 76.28±0.57 | 79.17±0.50         | 78.77±0.37           |
|              | CIFAR-100-C | 52.56±0.12 | 68.03±0.30         | <b>69.60</b> ±0.68   |

Table 2: Classification accuracy on clean CIFAR-10/CIFAR-100 datasets and Mean Corrupted Accuracy (mCA) on corrupted CIFAR-10-C/CIFAR-100-C datasets for ResNet-18, DenseNet-121 and Inception-V3 architectures. MAGNMA achieves a large/moderate mCA gain in comparison to Standard/AugMix training.

| Corruption        | Standard   | AT         | TRADES     | RSE        | GN         | AugMix             | MAGNMA <sub>oo</sub> | MAGNMA <sub>oo</sub> | MAGNMA <sub>oo</sub> |
|-------------------|------------|------------|------------|------------|------------|--------------------|----------------------|----------------------|----------------------|
| Clean             | 94.79±0.47 | 85.83±0.24 | 85.10±0.97 | 90.81±0.25 | 91.84±0.27 | 95.33±0.40         | 93.70±0.34           | 95.47±0.16           | 95.14±0.17           |
| mCA               | 77.83±0.11 | 78.89±0.27 | 74.57±1.16 | 84.09±0.44 | 85.47±0.58 | 89.70±0.40         | 87.14±0.48           | 89.66±0.32           | <b>91.46</b> ±0.28   |
| Brightness        | 93.97±0.52 | 84.72±0.26 | 83.20±1.09 | 89.71±0.29 | 90.42±0.39 | 94.73±0.41         | 92.71±0.42           | <b>95.08</b> ±0.16   | 94.80±0.17           |
| Contrast          | 82.78±1.19 | 52.84±0.84 | 40.70±1.49 | 63.96±0.56 | 70.75±1.49 | 93.11±0.59         | 74.57±0.98           | <b>94.08</b> ±0.22   | 93.51±0.42           |
| Defocus Blur      | 83.08±0.31 | 81.84±0.37 | 77.51±1.18 | 85.97±0.37 | 85.99±0.54 | <b>93.80</b> ±0.56 | 87.12±0.51           | 93.62±0.15           | 93.64±0.23           |
| Elastic Transform | 85.34±0.45 | 80.43±0.40 | 75.76±1.32 | 84.63±0.38 | 85.41±0.59 | <b>90.78</b> ±0.40 | 86.61±0.50           | 89.78±0.13           | 90.52±0.29           |
| Fog               | 90.33±0.62 | 67.02±0.71 | 54.91±2.17 | 72.89±0.35 | 77.64±0.84 | 92.15±0.72         | 83.65±0.52           | <b>92.50</b> ±0.42   | 92.24±0.38           |
| Frost             | 81.07±0.09 | 80.84±0.30 | 76.23±1.37 | 86.89±0.48 | 87.80±0.55 | 89.95±0.51         | 90.10±0.65           | 89.82±0.39           | <b>92.27</b> ±0.36   |
| Gaussian Blur     | 75.42±0.12 | 80.11±0.39 | 74.50±1.21 | 83.79±0.40 | 83.14±0.61 | <b>92.78</b> ±0.56 | 83.78±0.57           | 92.37±0.18           | 92.74±0.34           |
| Glass Blur        | 51.90±0.71 | 79.83±0.37 | 73.73±1.24 | 82.02±0.65 | 82.30±1.13 | 78.99±0.22         | 82.83±0.18           | 73.89±1.19           | <b>84.21</b> ±0.38   |
| Impulse Noise     | 57.18±1.57 | 76.61±1.20 | 73.19±0.48 | 83.83±0.96 | 89.20±0.37 | 84.98±0.30         | 89.71±0.48           | 86.24±1.10           | <b>89.86</b> ±0.22   |
| JPEG Compression  | 81.02±0.01 | 83.97±0.24 | 81.83±0.95 | 88.82±0.38 | 89.57±0.35 | 88.29±0.20         | <b>89.96</b> ±0.41   | 89.22±0.14           | 89.79±0.22           |
| Motion Blur       | 78.52±0.95 | 78.32±0.43 | 71.68±1.18 | 81.58±0.39 | 80.34±0.90 | <b>91.34</b> ±0.48 | 81.43±0.69           | 90.48±0.47           | 91.10±0.27           |
| Pixelate          | 76.72±0.05 | 84.06±0.29 | 81.70±1.15 | 88.53±0.33 | 88.78±0.49 | 84.38±0.62         | <b>89.64</b> ±0.24   | 86.20±0.90           | 88.23±0.51           |
| Saturate          | 92.35±0.53 | 82.28±0.41 | 82.28±1.11 | 87.00±0.40 | 88.05±0.44 | 93.00±0.46         | 90.71±0.59           | <b>93.86</b> ±0.15   | 93.47±0.25           |
| Shot Noise        | 59.51±1.65 | 81.57±0.47 | 80.52±0.86 | 89.22±0.48 | 90.51±0.33 | 85.01±0.29         | <b>91.91</b> ±0.41   | 85.58±0.35           | 91.78±0.34           |
| Snow              | 83.40±0.64 | 81.78±0.22 | 79.72±1.13 | 85.32±0.44 | 86.24±0.47 | 90.17±0.66         | 87.93±0.59           | 89.64±0.38           | <b>90.93</b> ±0.24   |
| Spatter           | 85.51±0.35 | 81.54±0.28 | 79.75±1.06 | 85.59±0.50 | 86.76±0.50 | 92.79±0.53         | 87.97±0.45           | <b>93.11</b> ±0.15   | 92.69±0.30           |
| Speckle Noise     | 62.90±1.52 | 81.03±0.40 | 79.86±0.98 | 88.85±0.50 | 90.60±0.31 | 85.82±0.40         | <b>91.96</b> ±0.39   | 86.41±0.41           | 91.86±0.32           |
| Zoom Blur         | 80.00±0.27 | 81.31±0.37 | 75.28±1.10 | 85.05±0.30 | 84.97±0.55 | 92.54±0.60         | 85.92±0.51           | 91.99±0.28           | <b>92.54</b> ±0.27   |

Table 3: Classification accuracy on CIFAR-10-C across different corruptions for various methods using a ResNet18 architecture. The best accuracy is highlighted in bold for each row which corresponds to a specific corruption. MAGNMA achieves the highest mCA score while maintaining high clean accuracy.

| Corruption        | Standard   | AT         | TRADES     | RSE        | GN                 | AugMix             | MAGNMA <sub>oo</sub> | MAGNMA <sub>oo</sub> | MAGNMA <sub>oo</sub> |
|-------------------|------------|------------|------------|------------|--------------------|--------------------|----------------------|----------------------|----------------------|
| Clean             | 76.60±0.15 | 59.72±0.52 | 59.83±1.18 | 66.59±0.26 | 67.24±0.58         | 76.44±0.34         | 73.29±0.11           | 77.44±0.29           | 76.79±0.07           |
| mCA               | 51.73±0.27 | 50.28±0.32 | 48.50±1.76 | 57.11±0.16 | 58.74±0.21         | 64.73±0.28         | 62.48±0.20           | 65.70±0.36           | <b>68.38</b> ±0.23   |
| Brightness        | 74.20±0.38 | 57.22±0.68 | 56.86±0.93 | 64.44±0.31 | 64.82±0.54         | 74.76±0.45         | 70.60±0.29           | <b>76.27</b> ±0.26   | 75.51±0.13           |
| Contrast          | 62.93±0.21 | 31.05±0.56 | 22.94±2.58 | 39.65±0.41 | 44.46±1.08         | 72.40±0.74         | 52.66±0.44           | <b>73.99</b> ±0.30   | 72.31±0.51           |
| Defocus Blur      | 58.87±0.38 | 53.82±0.35 | 51.84±2.29 | 59.32±0.21 | 59.28±0.14         | <b>73.34</b> ±0.35 | 61.86±0.18           | 72.83±0.09           | 72.89±0.26           |
| Elastic Transform | 60.36±0.34 | 52.05±0.36 | 49.91±2.39 | 57.60±0.15 | 57.91±0.34         | 67.25±0.13         | 61.52±0.03           | 66.81±0.33           | <b>67.25</b> ±0.10   |
| Fog               | 67.31±0.40 | 38.40±0.29 | 31.77±2.64 | 44.66±0.32 | 48.12±1.40         | 68.24±0.27         | 58.70±0.77           | <b>68.81</b> ±0.44   | 68.26±0.12           |
| Frost             | 50.76±0.40 | 51.39±0.88 | 48.46±1.00 | 60.07±0.30 | 61.06±0.28         | 63.04±0.54         | 66.43±0.33           | 63.66±0.78           | <b>68.50</b> ±0.59   |
| Gaussian Blur     | 49.75±0.53 | 51.79±0.44 | 49.12±2.43 | 56.45±0.23 | 56.21±0.59         | <b>71.39</b> ±0.28 | 57.22±0.34           | 70.07±0.08           | 70.52±0.19           |
| Glass Blur        | 21.89±0.21 | 51.48±0.74 | 49.14±2.49 | 54.38±0.10 | <b>55.60</b> ±1.10 | 40.65±0.13         | 53.90±0.71           | 35.87±2.17           | 53.66±1.19           |
| Impulse Noise     | 28.49±0.38 | 41.00±1.66 | 43.45±0.81 | 53.03±0.32 | 63.78±0.30         | 62.42±3.15         | 65.95±0.19           | <b>68.38</b> ±1.34   | 67.99±0.76           |
| JPEG Compression  | 51.74±0.43 | 57.03±0.54 | 55.90±1.80 | 63.65±0.14 | 63.92±0.34         | 60.57±0.01         | <b>65.60</b> ±0.36   | 64.17±0.46           | 64.56±0.39           |
| Motion Blur       | 54.26±0.95 | 50.33±0.51 | 47.00±2.65 | 54.25±0.19 | 54.11±0.66         | <b>69.28</b> ±0.06 | 56.31±0.33           | 67.18±0.29           | 68.70±0.20           |
| Pixelate          | 51.95±0.20 | 57.29±0.60 | 56.64±1.74 | 63.91±0.14 | 64.32±0.16         | 57.96±0.93         | <b>65.95</b> ±0.91   | 61.88±0.42           | 65.11±0.89           |
| Saturate          | 67.08±0.55 | 49.07±0.41 | 50.10±0.16 | 56.10±0.15 | 56.76±0.43         | 66.87±0.38         | 63.27±0.34           | <b>68.91</b> ±0.54   | 68.20±0.25           |
| Shot Noise        | 30.63±0.39 | 52.72±0.67 | 53.27±1.34 | 63.66±0.10 | 65.96±0.43         | 52.69±0.46         | <b>70.21</b> ±0.18   | 56.98±1.50           | 69.43±0.37           |
| Snow              | 56.17±0.28 | 53.57±0.83 | 52.27±1.27 | 58.56±0.11 | 59.13±0.19         | <b>67.17</b> ±0.42 | 62.47±0.19           | 65.81±0.09           | 67.10±0.44           |
| Spatter           | 59.70±0.38 | 52.77±0.68 | 52.82±1.42 | 57.56±0.08 | 58.63±0.22         | 72.31±0.58         | 62.84±0.31           | <b>73.18</b> ±0.39   | 71.51±0.25           |
| Speckle Noise     | 32.36±0.46 | 51.34±0.84 | 51.83±1.38 | 62.94±0.14 | 65.78±0.41         | 54.21±0.51         | <b>70.13</b> ±0.20   | 58.50±1.42           | 69.61±0.37           |
| Zoom Blur         | 52.64±0.46 | 52.72±0.32 | 49.62±2.67 | 57.68±0.33 | 57.54±0.39         | <b>70.52</b> ±0.07 | 58.94±0.37           | 69.22±0.13           | 69.79±0.04           |

Table 4: Classification accuracy on CIFAR-100-C across different corruptions for various non-hybrid methods using a ResNet18 architecture. The best accuracy is highlighted in bold for each row which corresponds to a specific corruption. MAGNMA achieves the highest mCA score while maintaining high clean accuracy.

## References

- A. Krizhevsky, I. Sutskever, and G. E. Hinton. Imagenet classification with deep convolutional neural networks. In *Advances in Neural Information Processing Systems*, 2012.
- K. He, X. Zhang, S. Ren, and J. Sun. Delving deep into rectifiers: Surpassing human-level performance on imagenet classification. In *ICCV*, 2015.
- Yanping Huang, Youlong Cheng, Ankur Bapna, Orhan Firat, Mia Xu Chen, Dehao Chen, HyoukJoong Lee, Jiquan Ngiam, Quoc V. Le, Yonghui Wu, and Zhifeng Chen. Gpipe: Efficient training of giant neural networks using pipeline parallelism. In *NeurIPS*, 2019.
- Dan Hendrycks and Thomas Dietterich. Benchmarking neural network robustness to common corruptions and perturbations. In *ICLR*, 2019.
- L. Engstrom, B. Tran, D. Tsipras, L. Schmidt, and A. Madry. Exploring the landscape of spatial robustness. In *ICML*, 2019.
- A. Torralba and A. A. Efros. Unbiased look at dataset bias. In *CVPR*, 2011.
- B. Recht, R. Roelofs, L. Schmidt, and V. Shankar. Unbiased look at dataset bias. In *ICML*, 2019.
- A. Madry, A. Makelov, L. Schmidt, D. Tsipras, and A. Vladu. Towards deep learning models resistant to adversarial attacks. In *ICLR*, 2018.
- H. Zhang, Y. Yu, J. Jiao, E. P. Xing, L. El Ghaoui, and M. I. Jordan. Theoretically principled trade-off between robustness and accuracy. In *ICML*, 2019.
- A. Joshi, A. Mukherjee, S. Sarkar, and C. Hegde. Semantic adversarial attacks: Parametric transformations that fool deep classifiers. In *ICCV*, 2019.
- K. Xiao, L. Engstrom, A. Ilyas, and A. Madry. Noise or signal: The role of image backgrounds in object recognition. In *ICLR*, 2021.
- D. Kang, Y. Sun, D. Hendrycks, T. Brown, and J. Steinhardt. Testing robustness against unforeseen adversaries. In *arXiv pre-print arxiv:1908.08016*, 2019.
- R. Geirhos, C. R. M. Temme, J. Rauber, H. H. Schutt, M. Bethge, and F. A. Wichmann. Generalisation in humans and deep neural networks. In *NeurIPS*, 2018.
- S. Chun, S. J. Oh, S. Yun, D. Han, J. Choe, and Y. Yoo. An empirical evaluation on robustness and uncertainty of regularization methods. In *ICML Workshop on Uncertainty and Robustness in Deep Learning*, 2019.
- E. D. Cubuk, B. Zoph, D. Mane, V. Vasudevan, and Q. V. Le. Autoaugment: Learning augmentation strategies from data. In *CVPR*, 2019.
- Balaji Lakshminarayanan, Alexander Pritzel, and Charles Blundell. Simple and scalable predictive uncertainty estimation using deep ensembles. In *NeurIPS*, 2017.
- Dan Hendrycks, Kimin Lee, and Mantas Mazeika. Using pre-training can improve model robustness and uncertainty. In *ICML*, 2019.
- Yaniv Ovadia, Emily Fertig, Jie Ren, Zachary Nado D Sculley, Sebastian Nowozin, Joshua V Dillon, Balaji Lakshminarayanan, and Jasper Snoek. Can you trust your model’s uncertainty? evaluating predictive uncertainty under dataset shift. In *NeurIPS*, 2019.
- D. Hendrycks, N. Mu, E. D. Cubuk, B. Zoph, J. Gilmer, and B. Lakshminarayanan. Augmix: A simple data processing method to improve robustness and uncertainty. In *ICLR*, 2020.
- Dimitris Tsipras, Shibani Santurkar, Logan Engstrom, Alexander Turner, and Aleksander Madry. Robustness may be at odds with accuracy. In *ICLR*, 2019.
- X. Liu, M. Cheng, H. Zhang, and C.-J. Hsieh. Towards robust neural networks via random self-ensemble. In *ECCV*, 2018.
- T. DeVries and G. W. Taylor. Improved regularization of convolutional neural networks with cutout. In *arXiv:1708.04552*, 2017.
- Hongyi Zhang, Moustapha Cisse, Yann Dauphin, and David Lopez-Paz. mixup: Beyond empirical risk minimization. In *ICLR*, 2017.
- Yuji Tokozume, Yoshitaka Ushiku, and Tatsuya Harada. Between-class learning for image classification. In *CVPR*, 2018.

- Sangdoon Yun, Dongyoon Han, Seong Joon Oh, Sanghyuk Chun, Junsuk Choe, and Youngjoon Yoo. Cutmix: Regularization strategy to train strong classifiers with localizable features. In ICCV, 2019.
- Ekin Dogus Cubuk, Barret Zoph, Dandelion Mane, Vijay Vasudevan, and Quoc V. Le. Autoaugment: learning augmentation policies from data. In CVPR, 2018.
- S. Kullback. Information Theory and Statistics. Dover, 1997.
- Alex Krizhevsky, Vinod Nair, and Geoffrey Hinton. Cifar-10 and cifar-100 datasets, 2009. URL <https://www.cs.toronto.edu/~kriz/cifar.html>.
- K. He, X. Zhang, S. Ren, and J. Sun. Deep residual learning for image recognition. In CVPR, 2016.
- Gao Huang, Zhuang Liu, Laurens van der Maaten, and Kilian Q Weinberger. Densely connected convolutional networks. In CVPR, 2017.
- Christian Szegedy, Vincent Vanhoucke, Sergey Ioffe, Jonathon Shlens, and Zbigniew Wojna. Rethinking the inception architecture for computer vision. In arXiv:1512.00567v3, 2015.
- C. Lin, J. Martens, S. Gowal, D. Krishnan, K. Dvijotham, A. Fawzi, S. De, R. Stanforth, and P. Kohli. Adversarial robustness through local linearization. In NeurIPS, 2019.

## 7 Supplementary Material

### 7.1 Data Corruption Visualizations

An example image along with its corrupted versions is shown in Figure 4; although humans might be able to recognize this as a boat, a deep learning image classifier trained in a standard manner will fail against most of these corruptions.

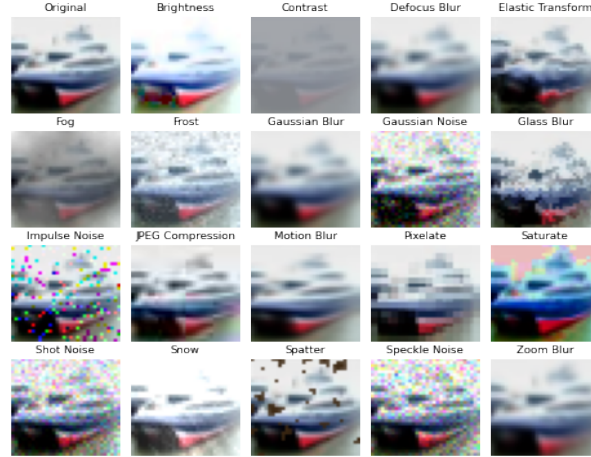


Figure 4: Example CIFAR-10 test image along with its corrupted versions. These corruptions are not available in the training process, and are only used for evaluation at inference time.

### 7.2 Proof of Proposition 1

**Proof:** From Appendix C in [Lin et al., 2019], the Hessian of the softmax cross-entropy function can be decomposed as:

$$H(x) = J^T(\text{diag}(p) - pp^T)J$$

where  $J$  denotes the Jacobian of the network function  $f_\theta$  (logits) and  $p$  denotes the softmax probabilities. The Jacobian transposed is denoted as  $J^T = [J_1^T, \dots, J_K^T]$  with  $J_k := \nabla_x f_k(x)^T$ . Starting from the FIM in (7), we have:

$$\begin{aligned} G_\theta(x) &= \sum_k p_k (\nabla_x \log p_k) (\nabla_x \log p_k)^T \\ &= \sum_k p_k (\nabla_x f_k - J^T p) (\nabla_x f_k - J^T p)^T \\ &= \sum_k p_k (\nabla_x f_k \nabla_x f_k^T - \nabla_x f_k p^T J - J^T p \nabla_x f_k^T + J^T p p^T J) \\ &= \sum_k p_k \nabla_x f_k \nabla_x f_k^T - \left( \sum_k p_k \nabla_x f_k \right) p^T J - J^T p \left( \sum_k p_k \nabla_x f_k \right)^T + J^T p p^T J \\ &= \sum_k p_k \nabla_x f_k \nabla_x f_k^T - J^T p p^T J - J^T p p^T J + J^T p p^T J \\ &= \sum_k p_k J_k^T J_k - J^T p p^T J \\ &= J^T \text{diag}(p) J - J^T p p^T J \\ &= J^T (\text{diag}(p) - p p^T) J \\ &= H(x) \end{aligned}$$

This concludes the proof. □

### 7.3 Proof of Theorem 1

**Proof:** Using the quadratic loss approximation near  $x$ , we have:

$$\mathcal{L}(x + \delta, y) = \mathcal{L}(x, y) + \delta^T \nabla_x \mathcal{L}(x, y) + \frac{1}{2} \delta^T H(x) \delta + o(\|\delta\|_2^2)$$

By using up to second order terms, an upper bound on the loss variation holds as:

$$\begin{aligned} |\mathcal{L}(x + \delta, y) - \mathcal{L}(x, y)| &\approx |\langle \nabla_x \mathcal{L}(x, y), \delta \rangle + \frac{1}{2} \delta^T H(x) \delta| \\ &\leq \|\delta\|_2 \cdot \|\nabla_x \mathcal{L}(x, y)\|_2 + \frac{1}{2} \delta^T H(x) \delta \end{aligned} \quad (13)$$

where we used the triangle inequality, and the Cauchy-Schwarz inequality to bound the linear term and the fact that  $H(x)$  is positive semidefinite. The gradient in the first term of (13) can be written as:

$$\begin{aligned} &\|\nabla_x \mathcal{L}(x, y)\|_2 \\ &= \sqrt{\left\| \sum_k -y_k \nabla_x \log p(x)_k \right\|_2^2} = \sqrt{\sum_k y_k \|\nabla_x \log p(x)_k\|_2^2} \\ &= \sqrt{\sum_k e_k \|\nabla_x \log p(x)_k\|_2^2 + \sum_k p(x)_k \|\nabla_x \log p(x)_k\|_2^2} \end{aligned}$$

where  $e_k = y_k - p(x)_k$  is the prediction error. The quadratic form in (13) can be upper bounded using the eigenvalue bound:

$$\delta^T H(x) \delta \leq \lambda_{\max}(H(x)) \|\delta\|_2^2$$

Using the two preceding bounds into (13), the desired bound (11) is obtained. The proof is complete.  $\square$

### 7.4 Experimental Results

**Robustness Results.** Figure 5 shows a comparison between clean accuracies on CIFAR-10 and mean corrupted accuracies on CIFAR-10-C for various deep learning methods using a ResNet-18 architecture. Figure 7 visualizes the corruption robustness profile over various corruption categories; it shows MAGNMA improves corruption robustness upon standard models by a large margin. Table 4 and Figures 8, 6 showcase additional results on the clean CIFAR-100 and corrupted CIFAR-100-C datasets for the same baselines on the ResNet-18 architecture. Compared to Standard training, MAGNMA achieves an mCA absolute improvement of 13.6%.

**Hyperparameter Sensitivity.** We study the effect of the training hyperparameters  $(\lambda_1, \lambda_2, \sigma_{\max}, \beta)$  on the robustness and uncertainty estimation performance of misclassification-aware Gaussian Noise and Mixed Augmentation (MAGNMA) training using the ResNet-18 architecture for CIFAR-10 dataset.

Table 5 contains the robustness and calibration results from which it is evident that the robustness and calibration performance is not too sensitive to the choice of hyperparameters as the clean accuracy, mCA, and RMSE calibration error do not change significantly.

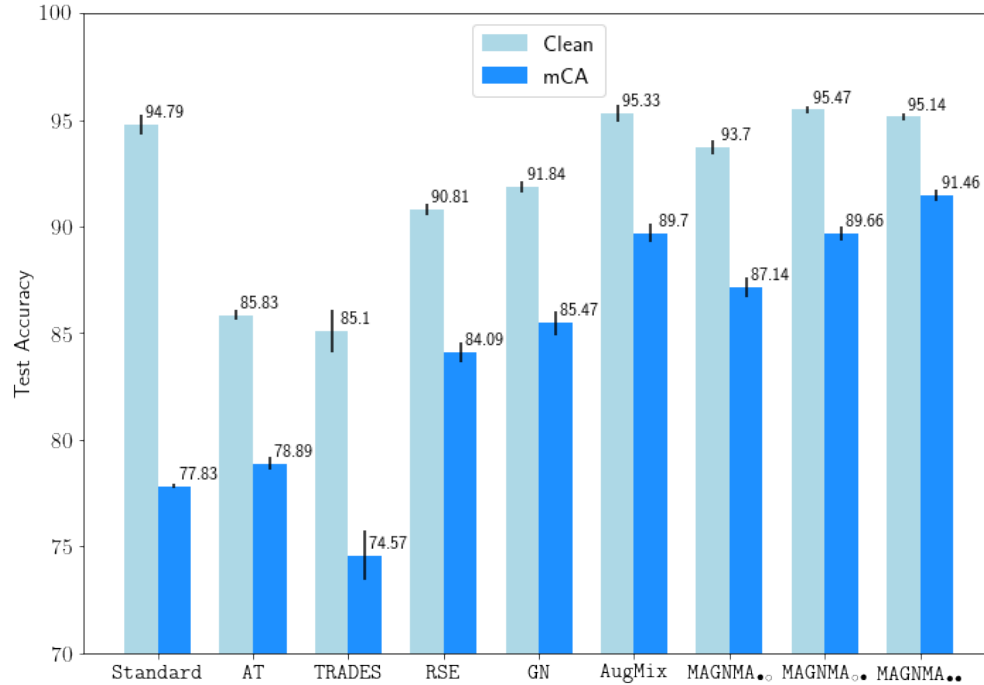


Figure 5: Clean and mCA performance on CIFAR-10 and CIFAR-10-C respectively for various deep learning methods. Our approach MAGNMA provides a significant robustness improvement in comparison to Standard training and outperforms all baselines.

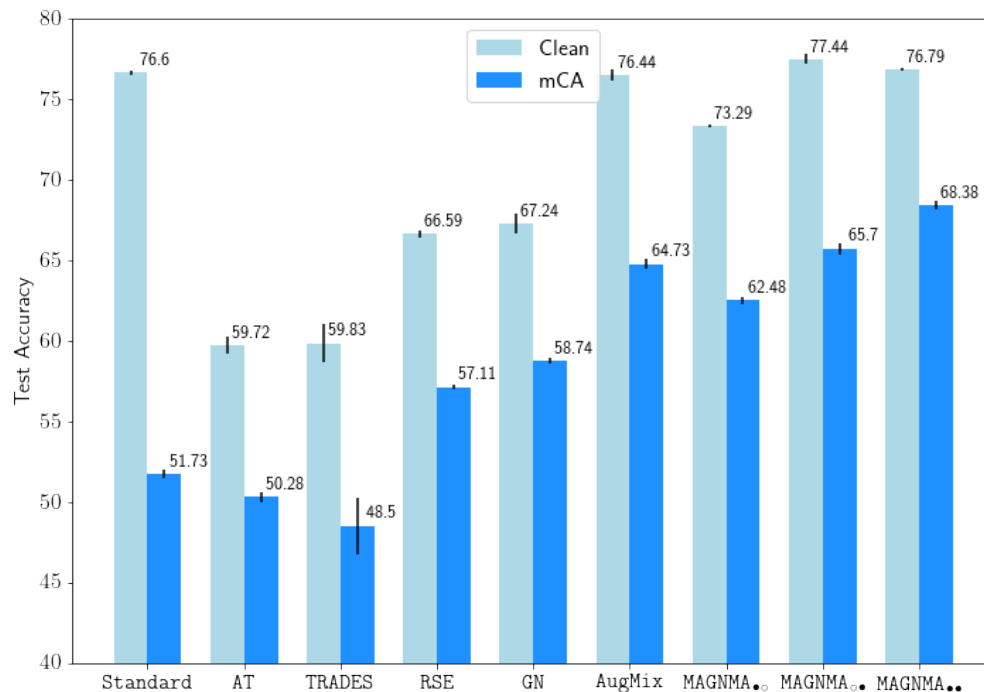


Figure 6: Clean and mCA performance on CIFAR-100 and CIFAR-100-C respectively for various deep learning methods. Similar to Figure 5 for CIFAR-10-C, our approach MAGNMA provides significant improvement in robustness over Standard training and outperforms all baselines.

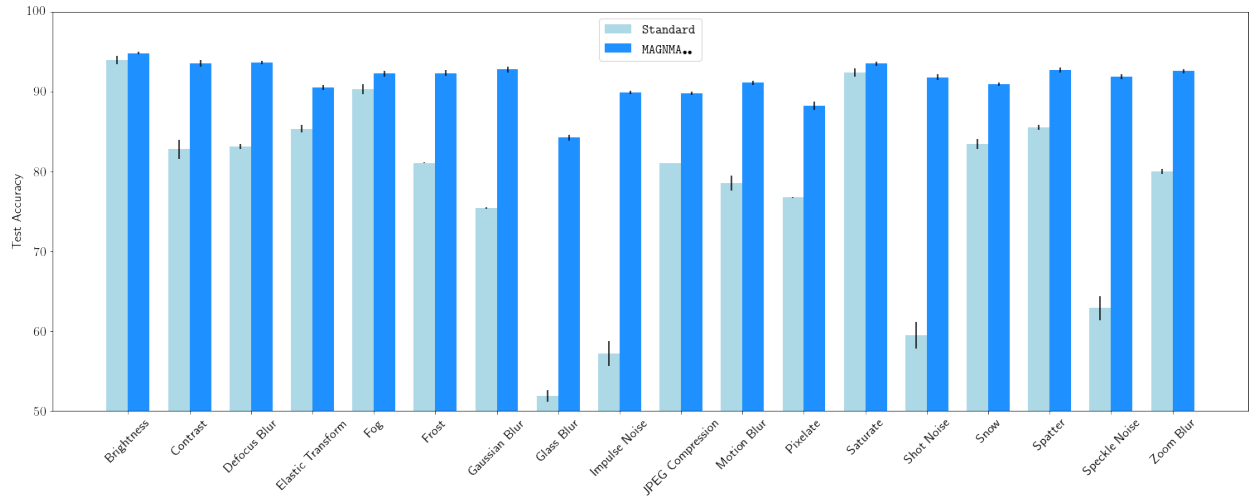


Figure 7: Robustness against a variety of corruptions including CIFAR-10-C weather, blur, noise and digital corruptions. Our approach MAGNMA improves robustness by a large margin despite not having seen these during training.

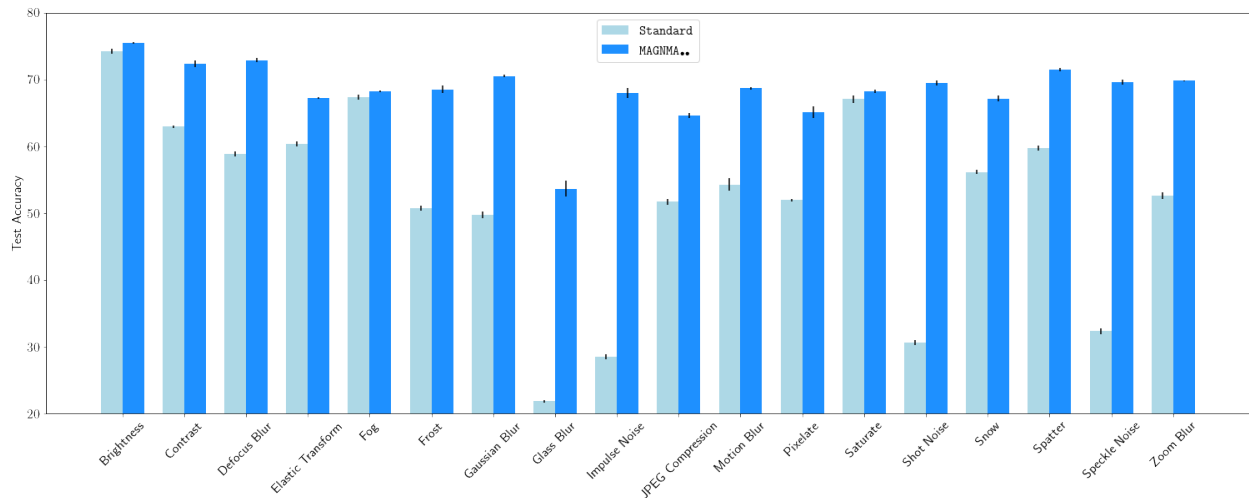


Figure 8: Robustness against a variety of corruptions including CIFAR-100-C weather, blur, noise and digital corruptions. Similar to the observed results on the CIFAR-10-C dataset, our approach MAGNMA yields significantly improved robustness.

| Parameters $(\lambda_1, \lambda_2, \sigma_{\max}, \beta)$ | Clean accuracy | mCA        | Clean RMSE | Corrupt RMSE |
|---|----------------|------------|------------|--------------|
| (0.1, 0, 0.2, 1)  | 93.66±0.44     | 86.24±0.41 | 5.08±0.58  | 8.97±0.37    |
| (0.1, 0, 0.25, 1)   | 93.45±0.26     | 86.33±0.71 | 5.18±0.15  | 9.09±0.64    |
| (0.15, 0, 0.2, 1)   | 93.80±0.39     | 86.93±0.56 | 5.32±0.18  | 9.12±0.36    |
| (0.2, 0, 0.2, 1)  | 93.70±0.34     | 87.13±0.48 | 4.86±0.54  | 8.85±0.34    |
| (0.3, 0, 0.2, 1)  | 93.55±0.19     | 87.11±0.35 | 4.84±0.21  | 8.71±0.21    |
| (0.4, 0, 0.2, 1)  | 93.32±0.11     | 86.74±0.29 | 4.96±0.41  | 8.67±0.13    |
| (0.5, 0, 0.2, 1)  | 92.96±0.26     | 86.38±0.38 | 4.79±0.24  | 8.48±0.09    |
| (0, 0.1, 0.2, 1)  | 95.11±0.37     | 89.27±0.61 | 2.36±0.19  | 5.74±0.35    |
| (0, 0.2, 0.2, 1)  | 95.34±0.24     | 89.53±0.47 | 1.89±0.29  | 5.59±0.37    |
| (0, 1.0, 0.2, 1)  | 95.30±0.27     | 89.66±0.30 | 2.01±0.04  | 5.21±0.15    |
| (0, 5.0, 0.2, 1)  | 95.47±0.16     | 89.66±0.32 | 1.67±0.25  | 4.80±0.26    |
| (0, 10.0, 0.2, 1)   | 95.15±0.20     | 88.97±0.24 | 2.02±0.35  | 3.10±0.66    |
| (0.2, 0.02, 0.2, 1)                                       | 95.10±0.25     | 91.23±0.41 | 1.95±0.17  | 3.43±0.34    |
| (0.2, 0.05, 0.2, 1)                                       | 95.08±0.25     | 91.04±0.30 | 2.03±0.29  | 3.02±0.52    |
| (0.2, 0.1, 0.2, 1)  | 94.93±0.40     | 91.12±0.35 | 1.88±0.32  | 3.16±0.26    |
| (0.2, 0.2, 0.2, 1)  | 95.01±0.34     | 90.90±0.49 | 1.91±0.17  | 3.00±0.59    |
| (0.2, 0.3, 0.2, 1)  | 95.14±0.17     | 91.46±0.28 | 1.69±0.04  | 2.96±0.47    |
| (0.2, 1.0, 0.2, 1)  | 95.30±0.36     | 91.38±0.51 | 1.42±0.12  | 2.98±0.18    |
| (0.2, 3.0, 0.2, 1)  | 95.33±0.20     | 91.31±0.33 | 1.36±0.08  | 2.95±0.42    |
| (0.2, 5.0, 0.2, 1)  | 95.46±0.08     | 91.19±0.32 | 2.20±0.73  | 1.70±0.65    |
| (0.2, 10.0, 0.2, 1)                                       | 95.22±0.28     | 91.13±0.20 | 1.48±0.20  | 2.07±0.51    |

Table 5: Sensitivity analysis on hyperparameters of MAGNMA training method. MAGNMA training was used with  $n = 5$  stochastic samples for each regularizer. Test set accuracy and RMS calibration error for CIFAR-10 and CIFAR-10-C datasets on ResNet-18 architecture are shown.